Article

Structural, Electronic, Magnetic, and Hyperfine Properties of V-doped SnO$_2$ (Sn$_{1−x}$V$_x$O$_2$, *x*: 0, 0.042, 0.084, and 0.125). A DFT-Based Study

H. H. Medina Chanduví, A. M. Mudarra Navarro, V. Bilovol, L. A. Errico,* and A. V. Gil Rebaza

Read Online

ACCESS | Metrics & More | Article Recommendations

ABSTRACT: *Ab initio* electronic structure calculations were performed to study the effect of V-doping on the structural, electronic, and magnetic properties of tin dioxide (Sn$_{1−x}$V$_x$O$_2$, *x*: 0.042−0.125). Calculations have been performed using pseudopotentials and plane-wave and full potential linearized augmented plane-wave methods. State-of-the-art Heyd−Scuseria−Ernzerhof (HSE06) exchange−correlation hybrid functional and the Tran−Blaha-modified Becke−Johnson (TB-mBJ) exchange potential were employed. Our calculations showed that V^{4+} substitutionally replaces Sn^{4+} ions inducing a reduction of the volume cell of SnO$_2$ and shortening of the metal−oxygen nearest neighbor bond lengths. Spin polarization at the V sites is predicted. Our results indicate that the magnetic ground state of the resulting system is paramagnetic. TB-mBJ and HSE06 accurately describe the experimentally reported dependence of the band gap with *x*. Our theoretical results for the hyperfine parameters at the Sn sites are in excellent agreement with Mössbauer experiments. Hyperfine parameters at the V sites are also presented.
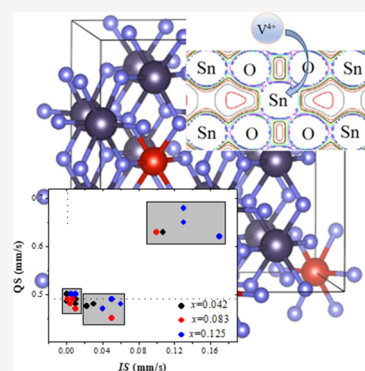
1. INTRODUCTION

The search and development of new materials with superior physical properties than those already known has always been preponderant for the development of our society. Particularly, from the middle of the 20th century, the demands for new materials increased and only high-tech materials could meet the new requirements: the new materials must be stronger, lighter, or present new electrical, electronic, optical, or magnetic properties for technological applications in different fields. These requirements give rise to an impressive development of materials: ceramics, metals, semiconductors, polymers, composite materials, superconductors, and so forth.

It is well known that defects play a fundamental role in the origin of the different physical properties of materials. For example, doping (under controlled conditions) can change the volume cell, induce deformations or break the crystal symmetry, and alter the electronic structure and the magnetic properties of the undoped material, giving rise to new functionalities.[1−7] Then, the understanding of the relation defect-properties and the capability to predict the physical properties accurately is fundamental for the development of new materials.[3−5] For this reason, computational methods have become an increasingly useful tool in material science.

Among the universe of materials, oxides exhibit unique structural, electronic, and magnetic properties and possess an exceptional potential as base materials in a broad range of industrial and technological applications including optical, electronic, optoelectronic, and biological fields.[8−10] Partic-

ularly, rutile-type tin dioxide (SnO$_2$) is maybe one of the most studied metallic oxide[11,12] and have attracted a renewed interest.[13−22] SnO$_2$ is a direct *n*-type semiconductor (a band gap of 3.6 eV, refs 14 and 23) that presents high electrical conductivity and transmittance in the ultraviolet−visible region and infrared reflectance.[24,25] Its n-type electrical conductivity is originated by intrinsic defects (oxygen vacancies and tin interstitials). The occurrence of transparency and conductivity makes it a suitable candidate for application as an optically passive component in optoelectronic devices such as solar cells,[26,27] touch screens,[28] transparent electrodes,[14] solid-state chemical and gas sensors,[11,29] catalytic support,[30] secondary lithium battery electrodes,[31] and potential candidates for spintronic devices.[15−22,32−34]

SnO$_2$ is a material that can be easily doped with a variety of impurities, and it was shown that the properties of SnO$_2$ nanostructures can be handled by doping it with adequate impurities.[22,35] SnO$_2$ nanoparticles have been successfully doped with transition-metal ions (V, Fe, Co, Mn, and Cu).[36−43] In particular, V-doping is expected to have significant effect on optical response[25,44,45] of SnO$_2$ (the
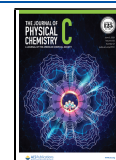
name "vanadium" is originated in the mythological Scandinavian god Vanadis because of its multicolored compounds), its electronic and catalytic properties,[25,44] and it can induce a ferromagnetic response at high temperature.[17,18,20,22]

Based on the previous discussion, it is clear that a realistic calculation could be of great interest to unravel the electronic structure of the SnO_2-doped system and obtain a better interpretation of the experimental results. Also, an accurate prediction of the electronic and structural effects induced by the V-dopant in the SnO_2 host lattice as a function of the V-concentration could be of great importance for the development of materials with new functionalities. Motivated by all these points, we present here a density functional theory (DFT)-based calculations of V-doped SnO_2 ($Sn_{1-x}V_xO_2$) for different V-concentrations (x) in the range 0.042−0.125, compositions that are in the range of the reported experimental studies. For each composition, we considered different distribution of the impurities in the host lattice and also different parallel/antiparallel spin alignments of the V impurities and we determined the structural, electronic, and magnetic properties of $Sn_{1-x}V_xO_2$ (lattice parameters a and c, c/a ratio, oxidation state of the V ions, band gaps, and magnetic moments) and the hyperfine parameters at the Sn sites. All these theoretical results are compared with different experimental ones. We also report the hyperfine parameters at the V sites.

This paper is organized as follows. In Section 2, we present the theoretical methods and the technical details of our calculations, the strategy used in our study and the supercell (SC) employed for the simulation of the different compositions considered. In Section 3, we present our first results: the magnetic moments at the V sites, the spin alignment when two or three impurities are introduced in SnO_2, and a discussion related to the oxidation state of V in SnO_2. In Section 3.2 we discuss our results for the structural parameters as a function of x and in Section 3.3, the band gap predicted by each approximation for the exchange and correlation (XC) potential. In Section 3.4, the hyperfine parameters at the Sn and V sites are presented, discussed, and compared with [119]Sn-Mössbauer experimental results. Finally, in Section 4, we present our conclusions.

2. THEORETICAL METHODOLOGY

The main goal of this work is to obtain from *ab initio* calculations the electronic structure of V-doped SnO_2 ($Sn_{1-x}V_xO_2$) for V-concentrations in the order of those reported in the literature and the structural, electronic, and hyperfine properties of the system under study.

Tin dioxide (stannic oxide or cassiterite) is a n-type wide-gap semiconductor with a direct band gap in the order of 3.6 eV[14,23] that crystallizes in the rutile structure with a flat (c/a = 0.672, refs 46 and 47) tetragonal unit cell (space group $P4_2/mnm$, no. 136). Lattice parameters (experimentally obtained, refs 46 and 47 and theoretical optimizations, refs 13, 48−51) are presented in Table 1. Other experimental and theoretical results for the lattice parameters can be found in ref 51. Rutile SnO_2 contains two molecules per unit cell with the Sn atoms located at Wyckoff positions 2a (0, 0, 0; 1/2, 1/2, 1/2) and the O atoms at positions 4f: ±(u, u, 0; 1/2+ u, 1/2− u, 1/2) with u in the range 0.3056−0.3064 (see Table 1). The Sn cations are surrounded by six O atoms as first-nearest neighbors (ONN) that form a slightly distorted octahedron with a rectangular basal plane of four ONN (ONN1 in the following) and two

Table 1. Experimental (refs 46 and 47) and Predicted (FP-LAPW and PP-PW Calculations, refs 48−51) Lattice Parameters a and c and Internal Structural Parameter u (This Parameter Defines the Position of the Oxygen Atoms in the Rutile Structure of Pristine SnO_2

oxide	FP-LAPW	PP-PW	experimental
SnO_2	a = 4.7710 Å	a = 4.728 Å	a = 4.7374$_1$ Å
	c = 3.1999 Å	c = 3.171 Å	c = 3.1864$_1$ Å
	u = 0.3056	u = 0.3050	u = 0.3056$_1$−0.3064$_4$

axial ONN (ONN2). The bond lengths Sn-ONN1 and Sn-ONN2 are 2.06 Å and 2.05 Å, respectively.

In our problem, we are dealing with a doped system. To reproduce the experimental V-concentrations we build a 72-atom SC with dimensions $2a \times 2a \times 3c$. The V-concentration (x) has been simulated replacing one, two, or three Sn atoms by V. In this way, the obtained V-concentrations are 0.042, 0.084, and 0.125, very close to the experimental ones (x = 0.05, 0.075, and 0.125, see e.g., refs 44 and 45). In the case of two or three impurities, every possible non-equivalent distribution of the impurities in the SC was calculated taking into account the changes in the volume cell and the internal structural distortions induced by the V impurities. Since it was reported previously that the V impurities could be polarized up to 1.0 μ_B,[17,18,20] spin-polarized calculations were performed considering different collinear spin configurations. The energy of each V-distribution and spin configuration was determined to obtain the structural and magnetic ground state for each x value.

The electronic structure of $Sn_{1-x}V_xO_2$ was determined by means of DFT[52]-based calculations. The self-consistent Kohn−Sham equations were solved using two complementary methods, pseudopotential and plane-wave (PP-PW) as implemented in the Quantum-Espresso code[53] and the full potential linearized augmented plane-wave method (FP-LAPW)[54,55] using the wien2k implementation of the method.[56] PP-PW was used to determine, for each V-concentration, the lower energy V-distribution and spin configuration and the volume changes induced by the impurities. The lower energy structure for each x value was used as input data for the FP-LAPW calculations. Using FP-LAPW, we obtained the electronic properties of the system and the hyperfine parameters at the Sn and V sites.

In the case of the PP-PW scalar relativistic calculations the ionic cores of the Sn, O and V atoms were described using ultrasoft pseudopotential from the standard solid-state pseudopotential library, SSSP.[57] The kinetic energy cutoff for the wave-function and charge density were set to 1088 and 10,880 eV, respectively. Variable-cell relax calculations were performed for the optimization of the volume cell and the atomic positions. The adopted cutoff convergence criterion for the structural minimization was forces on each ion smaller than 0.025 eV/Å and a residual stress on the cell below 0.1 kbar. The reciprocal space was described using a dense mesh-grid of 100 k-point to sample the first Brillouin zone. However, scalar relativistic FP-LAPW calculations were performed considering muffin-tin radii for Sn, V, and O of 1.11, 1.01, and 0.85 Å, respectively. The basis set was composed by more than 8800 plane waves plus 644 local orbitals ($R_{MT}xK_{max}$ = 7, being R_{MT} the smallest muffin-tin radius and K_{max} is related with the plane-wave cutoff). The same dense k-points mesh mentioned before was used in the FP-LAPW calculations.

In both calculations, the XC potential was described using two parameterizations of the generalized gradient approximation (GGA), the Wu and Cohen (WC-GGA, ref 58) and the Perdew−Burke−Ernzerhof (PBE-GGA, ref 59). Also, for checking purposes, the local spin-density approximation (LSDA, ref 60) was employed. Since all these approximations yield very similar results, we will concentrate our discussion on the WC-GGA results. To improve the description of the electronic structure of the $Sn_{1−x}V_xO_2$ system, we performed calculations considering XC potentials beyond GGA, the Heyd−Scuseria−Ernzerhof (HSE06) hybrid functional[61,62] and the Tran−Blaha-modified Becke−Johnson (TB-mBJ) exchange potential.[63] HSE06 is a state-of-the-art XC functional and one of the most accurate and precise XC potentials for the determination of band gaps. However, this approach is computationally expensive and time demanding. On the other hand, the TB-mBJ potential predicts band gaps with an accuracy comparable to hybrid functional in a wide range of semiconducting and insulating compounds but is less expensive in time and computational resources. The HSE06 and TB-mBJ calculations were performed considering only the lowest energy structures predicted by WC-GGA for each V-concentration.

The determination of the hyperfine interactions at a given nuclear site enables the investigation of the structural, electronic, and the magnetic sub-nanoscopic environment of this nuclear site.[64−66] In this work, two hyperfine parameters are determined and compared with experimental results obtained using ^{119}Sn-Mössbauer spectroscopy: the isomer shift (IS), which provides information on the local chemical bonds and the oxidation state of the Mössbauer probe and the quadrupole splitting (Δeq) that reflects the asymmetry of the electronic charge distribution around the Mössbauer probe nucleus. In the case of the ^{119}Sn probe, the IS is related to the electron density at the nucleus of the probe by[66]

$$IS = \alpha(\rho(0)_A - \rho(0)_R) \tag{1}$$

$\rho(0)_A$ and $\rho(0)_R$ are the electronic charge densities at the Sn nuclei in two different solid-state environments, the absorber (here, $Sn_{1−x}V_xO_2$) and the Sn sites of a reference material (SnO_2 in the present study), respectively. α is a calibration constant. In the case of the FP-LAPW method, the nucleus is modeled by a point-charge, and $\rho(0)_A$ and $\rho(0)_R$ are calculated at a point located at a distance R_0 from the nuclear site. In our work, we take $R_0 = 0.00001$ a.u. To obtain the IS, $\rho(R_0)_A$ and $\rho(R_0)_R$ must be computed using the same R_0 value. Additionally, $[\rho(R_0)_A - \rho(R_0)_R]$ could depend on the choice of R_0. For this reason, α must be determined for the R_0 value selected for the calculations. α was obtained by calculating $\rho(R_0)_A$ (with the same precision and the same parameters used in the case of calculations performed for $Sn_{1−x}V_xO_2$) in different tin compounds for which accurate experimental determinations of the IS (IS^{exp}) are reported in the literature. From a linear regression of $[\rho(R_0)_A - \rho(R_0)_R]$ versus IS^{exp} data, we obtained $\alpha = 0.068$ a.u.^{3} mm/s for the 23.875 keV excited state of ^{119}Sn. The same R_0 value and methodological considerations were considered in the calculation of $\rho(R_0)$ at the V sites that we will discuss in the next section.

The quadrupole splitting Δeq is originated in the (hyperfine) interaction of the nuclear quadrupole moment of the probe nucleus with the extra-nuclear crystalline potential. For a transition from $I = 3/2$ to $I = 1/2$, as in the case of the ^{119}Sn-Mössbauer probe, Δeq is given by[66]

$$\Delta eq = \frac{eQ}{2} V_{ZZ}\left(1 + \frac{\eta^2}{3}\right)^{1/2} \tag{2}$$

Here, $Q = 0.109$ b is the nuclear quadrupole moment of the 23.875 keV excited state of ^{119}Sn. V_{ZZ} is the largest eigenvalue of the diagonalized electric field gradient (EFG) tensor. The EFG tensor is a rank 2 traceless symmetric tensor whose components V_{ij} are defined by the second derivative of the Coulomb potential $V(\boldsymbol{r})$ with respect to the spatial coordinates. The three V_{ii} components of the eigenvalues of the EFG tensor are labelled according to the convention $|V_{zz}| < |V_{yy}| < |V_{zz}|$, and η is the asymmetry parameter defined as

$$\eta = \frac{V_{XX} - V_{YY}}{V_{ZZ}} \tag{3}$$

Finally, to study the precision of our PP-PW and FP-LAPW results, we performed several additional calculations, following the procedure described by some of us in ref 67. By examining the effect of different basis sets and k-point samplings, we conclude that for the parameters reported previously, our results are very well converged (relative numerical errors smaller than 2%).

3. RESULTS AND DISCUSSION

3.1. Preliminary Results: Magnetic Moments, Magnetic Configuration, and Charge State of the V Impurities in SnO$_2$. Before discussing our results for the structural, electronic, and hyperfine properties of V-doped SnO_2, we will present some important results. As we mentioned in Section 2, to simulate the experimental concentrations we replace one, two, or three Sn atoms by V ones. For the last two cases, we study all the possible inequivalent distributions of the V impurities in the host lattice. Spin-polarized and non-spin-polarized calculations were performed, taking into account the volume changes and the structural distortions induced by the impurities. After the analysis of the whole set of calculations, we conclude that irrespective of the V-concentration and distribution, the spin-polarized solutions have lower energy than the non-spin-polarized ones, so we will concentrate the discussion on these cases. Spin polarization comes mainly from the V-dopant [$\mu(V) = 0.85$ μ_B per V atom]. The contribution of the V-ONN atoms is very small ($\mu(ONN)$ in the order of 0.02 μ_B per ONN atom) and Sn remains non-polarized. The total magnetic moment for the 72-atom SC is 1.00 μ_B when one V impurity replaces a Sn atom. All these results are in very good agreement with those previously reported by Wang et al.[17,18] and Roy et al.[22]

When one vanadium atom substitutionally replaces a Sn one in the SC, the spin configuration of the doped system is forced to be ferromagnetic. However, in the case of two or three V-dopants, the lower energy collinear spin configuration must be determined. In the case of two V impurities, to determine the stability of the magnetic phases, we calculated the total energy of the antiferromagnetic state (E^{afm}) and the ferromagnetic state (E^{fm}) for all the possible V distributions and we evaluated the energy difference $\Delta E = E^{afm} - E^{fm}$ for each V distribution. Using this definition for ΔE, a negative ΔE value means that the magnetic ground state is antiferromagnetic, whereas a positive ΔE value means that the ferromagnetic spin alignment is the magnetic ground state. Irrespective of the V distribution (in other words, irrespective of the V−V separation in the 72-

atom SC), we obtained that the antiferromagnetic (afm) solutions have lower energy than the ferromagnetic (fm) ones. However, ΔE is around −1 meV per formula unit (f.u.). This energy difference is in the order of our convergence error for the energy differences, so both afm and fm configurations can be considered as degenerate solutions even for the smaller V−V separation. This result suggests that the direction of the local magnetic moments is random, resulting in a zero total magnetization and a paramagnetic ground state of $Sn_{1-x}V_xO_2$ for $x = 0.084$. These results are in perfect agreement with those reported by Salmani et al.[20] and Roy et al. (ref 22. Only a V−V separation of 6.7 Å was considered) and Wang et al.[17,18] In the later work, only two configurations were studied: one of these corresponds to the case when the V impurities are as close as possible and the second one corresponds to V atoms being as far as possible in the $2a \times 2a \times 2c$ (48 atoms) SC used (refs 17 and 18).

In the case of three V impurities in the 72-atom SC ($x = 0.125$), we studied the ferromagnetic state and different ferrimagnetic configurations. Again, ΔE is smaller than the convergence error, irrespective of the V distribution and magnetic configurations also indicating that the magnetic ground state of V-doped SnO_2 is paramagnetic. It is important to mention that our calculations only indicate that the ground state of $Sn_{1-x}V_xO_2$ could be paramagnetic. The magnetic state cannot be determined by only performing DFT calculations, and thus, further models are required. In ref 20 the stable magnetic state of $Sn_{1-x}M_xO_2$ (M: V, Cr, Mn, and Fe) was determined by comparing the total energy of different spin configurations assumed for $Sn_{1-x}M_xO_2$. These configurations were mapped to a classical Issing spin Hamiltonian to obtain the exchange couplings. The obtained exchange couplings were then used as input data in finite-temperature Monte Carlo simulations to obtain the thermal dependence of the total magnetization, the magnetic susceptibility, and the Curie temperature of $Sn_{1-x}M_xO_2$. The obtained Curie temperature of $Sn_{1-x}V_xO_2$ is in the order of 0 K, showing that ferromagnetic behavior is not expected even at 0 K for V-doped SnO_2.

We must remark here that the results for the structural, electronic, and hyperfine properties at the Sn and V sites that we will discuss in the following sections are those obtained for the lowest energy structures for each V-concentration, but the results are irrespective of the V distribution and the spin configuration.

Now we will discuss the charge state of the V impurities in rutile SnO_2. The structural and electronic properties of $Sn^{4+}O_2^{2-}$ doped with different impurities (with donor or acceptor character) were studied both theoretically and experimentally in different papers. Yahla et al.[68] performed a DFT-based study of Sb-doped SnO_2. Sb ions have often two oxidation states, 3+ and 5+. In most cases, only the Sb^{5+} oxidation state was observed. When both oxidation states are observed, their relative ratio depends on the synthesis process and characteristics of the samples.[68] Based on experimental results, it is assumed that the Sb^{5+} oxidation state corresponds to the cases in which Sb substitutionally replaces Sn in the bulk material and Sb^{3+} to the substitutional replacement of superficial Sn atoms. From the comparison of DFT−Mössbauer experimental results, Yahla et al. confirmed that in bulk SnO_2 samples, Sn^{4+} atoms are replaced by Sb^{5+}. On the other hand, some of us studied the case of Fe and Co in SnO_2,[39,41] ions that present oxidation states 2+ and 3+. In those studies, we have demonstrated that oxygen vacancies are

spontaneously formed in the first coordination shell of the impurities. By comparing theory−experiment, we also concluded that Fe^{3+} and Co^{3+} substitutionally replace Sn^{4+} in SnO_2.

Vanadium presents multiple oxidation states: 2+, 3+, 4+, and 5+. A reasonable hypothesis is that the oxidation state of V substitutionally located at Sn sites of SnO_2 is 4+. To confirm this point, we determined by means of Bader analysis[69] the electronic charge in the muffin-tin spheres of Sn and O atoms in pristine $Sn^{4+}O_2^{2-}$. We obtained $46.10e$ and $7.20e$ for Sn and O atoms, respectively. In the case of V-doped $Sn^{4+}O_2^{2-}$ these charges are, on average, $46.10e$ and $7.20e$ with a dispersion of $0.01e$, irrespective of the V-concentration and distribution in the host lattice. This result shows that the substitution of a Sn atom by V impurities does not produce changes in the charge in the Sn and O muffin-tin spheres, confirming that the oxidation states of Sn and O ions in V-doped SnO_2 are still 4+ and 2− even for the Sn and O atoms that are nearest neighbors of the V impurities. In the case of the charges in each V muffin-tin sphere, we obtained $20.28–20.29e$. After that, we studied the charge at the V sites in different V-oxides, namely, $V^{2+}O^{2-}$, r-$V^{4+}O_2^{2-}$ (rutile phase), m-$V^{4+}O_2^{2-}$ (monoclinic phase), $V_2^{3+}O_3^{2-}$, and $V_2^{5+}O_5^{2-}$. These oxides were studied using the same convergence criteria and R_{MT} that those used in the case of V-doped SnO_2. The structural data used in these calculations are reported in refs 70−73. By inspecting Table 2, we see that the charges in the V muffin-tin spheres for the

Table 2. Nominal Charge State and Electronic Charge in the Muffin-Tin Sphere of V in Different Vanadium Oxides and $Sn_{1-x}V_xO_2$

oxide	V nominal oxidation state	charge inside the V muffin-tin sphere
VO	2+	$20.54e$
V at the interstitial site in SnO_2		$20.54e$
V_2O_3	3+	$20.38e$
V in SnO_2 with one oxygen vacancy in its ONN shell		$20.36e$
m-VO_2	4+	$20.31e$
r-VO_2	4+	$20.30e$
$Sn_{1-x}V_xO_2$		$x = 0.0416, 20.28e$
		$x = 0.084, 20.29e$
		$x = 0.125, 20.28e$
V_2O_5	5+	$19.84e$

cases of r-$V^{4+}O_2^{2-}$ and m-$V^{4+}O_2^{2-}$ are $20.30e$, very similar to those of V at the cationic sites of SnO_2 ($20.28e$). From these results, we can conclude that the oxidation state of V in V-doped SnO_2 is 4+.

To confirm the charge state of V at cationic sites of SnO_2, we performed a second analysis. In Mössbauer experiments, the IS is a fingerprint of the oxidation state of the probe. Unfortunately, till date no Mössbauer results for V in SnO_2 are reported. In our approach, we will pay attention to $\rho(0)_A$, the electronic charge density at the nuclear site of the V impurity. The results obtained for $\rho(0)_A$ at V sites in different V-based oxides as a function of the nominal oxidation states are plotted in Figure 1. As can be seen, this linear correlation confirms that the oxidation states of V at cationic sites of SnO_2 is 4+. This conclusion is in perfect agreement with X-ray photoelectron spectroscopy performed in $Sn_{1-x}V_xO_2$ (x: 0.01, 0.03, and 0.05) nanoparticles synthesized by the combustion synthesis method that revealed the presence of vanadium as V^{4+} species in the
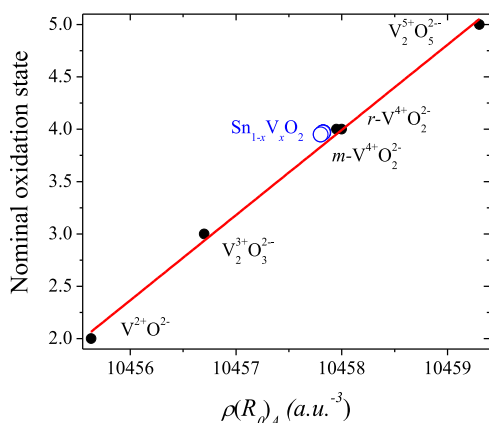
Figure 1. Nominal oxidation state of different vanadium oxides as a function of the electronic charge at the nucleus of the V atoms. Solid red line is the result of a linear fit to the data obtained in the WC-GGA calculations (excluding $Sn_{1-x}V_xO_2$).

SnO$_2$ host lattice.[74] A similar result was reported in ref 36 for other V-concentrations.

We also studied the possible formation of oxygen vacancies induced by the V-doping. Contrary to the case of Fe^{3+} and Co^{3+} impurities in SnO$_2$ (in which the impurities favor formation of oxygen vacancies in the ONN coordination shell of the impurities, refs 39 and 41), V excludes the oxygen vacancies. To determine the stability of the oxygen vacancies in the case of V-doped SnO$_2$, we calculate the formation energy $E(vac) = [E(red) + \mu(O)] - E(SC)$, where $E(red)$ and $E(SC)$ are the total energies of the SC containing one oxygen vacancy and the stoichiometric system, respectively. $\mu(O)$ is the chemical potential of the oxygen atom [we assumed that $\mu(O)$ is half the total energy of an oxygen molecule. Details of the calculation of $\mu(O)$ can be found in ref 41]. In the case of pure SnO$_2$, we obtained that the energy involved in the formation of an oxygen vacancy in the 72-atom SC is +4.4 eV (oxygen vacancy concentration: 2.1%). In the case of the doped system and for $x = 0.042$, we also obtained $E(vac) = +4.4$ eV. This result is irrespective of the localization of the oxygen vacancy (close to the substitutional V site or far away from this site). This result also supports the 4+ oxidation state for V in SnO$_2$. The magnetic moment at the V site in the presence of an oxygen vacancy is 0.85 μ_B, and the electronic charge in the muffin-tin spheres of a V atom with an oxygen vacancy in its ONN shell is 20.36e, a 3+ oxidation state (when the oxygen vacancy is generated in the second ONN shell, the electronic charge in the muffin-tin spheres of a V is 20.30e, a 4+ oxidation state, see Table 2).

In addition to the substitutional replacement of Sn atoms by V-dopants, we considered the formation of interstitial V sites in SnO$_2$. In this case, we first verified that the most stable position for an interstitial V atom is the octahedral site at the center of the (010) faces (atomic position: 0; 1/2; 1/2 in the primitive unit cell). In this site, an interstitial V-atom has six ONN: two O atoms at 1.72 Å and four at 2.34 Å. After the structural relaxation, the closest oxygen atoms relax outward from the interstitial site by 0.32 Å, while the other four O atoms are pulled in toward the interstitial V site by 0.18 Å (final V-ONN bond lengths at the interstitial site: 2.04 Å and 2.17 Å). The electronic charge in the muffin-tin spheres of the interstitial V atom is 20.53e that corresponds to V in a 2+ charge state (see

Table 2). A magnetic moment of 0.80 μ_B at the interstitial V site is obtained.

The formation of an interstitial V is found to be higher in energy, under all charge states, than a substitutional V. The formation energy of one interstitial V atom was calculated to be 8.0 eV, 1 order of magnitude larger than the substitution energy (the energies associated to the substitution of native Sn^{4+} atoms by V^{4+} are 0.48, 0.49, and 0.73 eV for $x = 0.042$, 0.84, and 0.125, respectively). Similar formation energies were found for the cases of interstitial Fe and Sn atoms in SnO$_2$ (refs 39 and 14, respectively).

3.2. Structural Properties. From the energy of all the V distributions in the SnO$_2$ host and spin configurations, we determined the equilibrium structures for each V-concentration x. In the case of $x = 0.042$, one V atom replaced the Sn atom located at the origin of coordinates (V1). For $x = 0.084$, the lowest energy structure corresponds to V ions located at $(0, 0, 0)$ and $(1/2, 0, 0)$, V1 and V2, respectively. In all the cases, the fractional coordinates of the V atoms correspond to the unrelaxed initial SC. The equilibrium V1−V2 separation is 4.753 Å (see Table 3). This study includes the cases of two V

Table 3. Equilibrium Structures of $Sn_{1-x}V_xO_2$ for the Different Concentrations x Studied[a]

x	V site (fractional coordinates)	V−V separation in the SC (Å)	magnetic moment at the V sites (μ_B)	V-ONN bond lengths (Å)
0.0416	V1: (0; 0; 0)		+0.84 (WC-GGA)	1.93^2/1.94^4
			+0.87 (TB-mBJ)	
0.083	V1: (0; 0; 0)	4.73	V1: +0.84 (WC-GGA)	V1: 1.93^2 /1.94^4
	V2: (1/2; 0; 0)		V2: −0.84 (WC-GGA)	V2: 1.93^2 /1.94^4
			V1: +0.86 (TB-mBJ)	
			V2: −0.86 (TB-mBJ)	
0.125	V1: (0; 0; 0)	V1−V2: 4.72	+0.83 (WC-GGA)	V1: 1.93^2 /1.94^4
	V2: (1/2; 0; 0)	V1−V3: 5.82	−0.84 (WC-GGA)	V2: 1.92^1 /1.94^1 /1.95^4
	V3: (1/4; 1/4; 1/2)	V2−V3: 5.82	−0.84 (WC-GGA)	V2: 1.92^1 /1.94^1 /1.96^4
			+0.87 (TB-mBJ)	
			−0.87 (TB-mBJ)	
			−0.87 (TB-mBJ)	

[a]In addition to the localization of the V impurities and impurity−impurity separations, the magnetic moments and the relative spin orientations (+/−, parallel/antiparallel spin orientations) and the V-ONN bond lengths are reported (in square brackets, we indicate the multiplicity).

atoms as close as possible (V−V separation: 3.12 Å) and farthest apart (7.42 Å for this 72-atom SC). If we set the energy of the equilibrium structure to 0, the energies of the closest and farthest V-configurations are +0.131 and +0.06 eV, respectively. As can be seen, the increase in the energy of the system is greater when the V-atoms get closer than when they move away. This result discards the formation of V-dimers.

In the case of three V in the 72-atom SC ($x = 0.125$), the lowest energy corresponds to V atoms located at V1: (0, 0, 0), V2: (1/2, 0, 0), and V3: (1/4, 1/4, 1/2). The V1−V2 separation is then 4.72 Å, and the V1−V3 and V2−V3

separations are 5.82 Å. All these results are resumed in Table 3. As in the case of two V atoms at cationic sites, from the study of the energy of the different V distributions of three V atoms, we refute the formation of V clusters.

As can be seen in Figure 2, the substitution of Sn^{4+} atoms by V^{4+} ones leads to a diminution of the volume cell. The
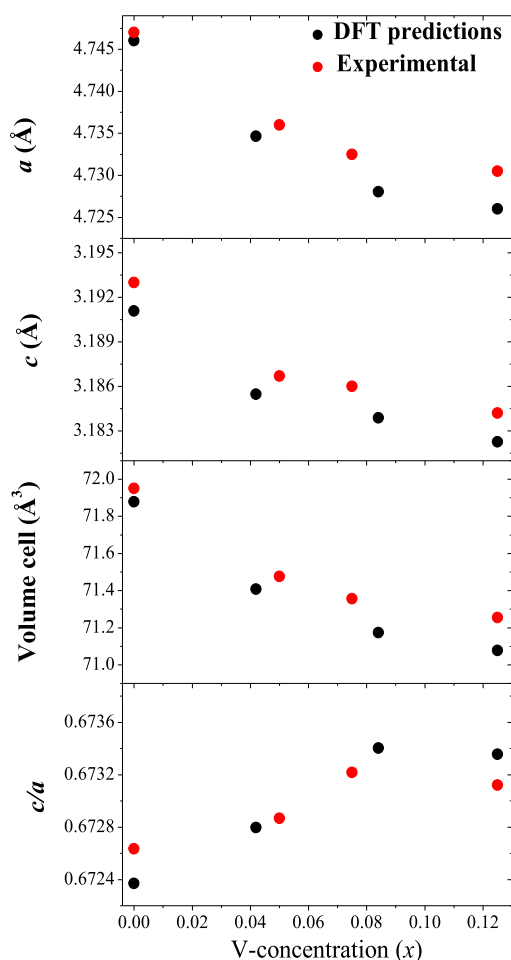

Figure 2. WC-GGA results for the lattice parameters a and c, volume cell, and c/a relation for $Sn_{1-x}V_xO_2$ as a function of the V-concentration x compared to the experimental results reported in ref 45.

impurity-induced volume reduction is symmetric in the sense that the tetragonal crystalline lattice symmetry of the SnO_2 host is retained, but the c/a ratio changes (a slight enlargement) with the V-concentration x (see Figure 2c). All these structural results are in excellent agreement with the reported experimental structural characterizations.[25,44,45,74,75]

In addition to the volume cell reduction and the change in the c/a relation, the incorporation of V-dopants into pure SnO_2 crystalline structure induces a relaxation of the ONN of V atoms. The computed atomic displacements are found to be inward with respect to the V ion giving rise to a decrease of about 0.1 Å for the six V-ONN bond lengths compared to the Sn-ONN bond lengths in pure SnO_2. It is important to mention here that the main structural effect of the substitution of Sn atom by V ones at concentrations lower than $x = 0.125$ is confined to the first V oxygen coordination shell. The magnitude of the structural relaxation rapidly decreases from the V-ONN to further shells (the displacement of the Sn-next

nearest neighbors to the V impurities is smaller than 0.02 Å). The origin of the defect-inward displacements of the V-ONN is the larger ionic radius of 6-fold coordinated Sn^{4+} ions (0.83 Å) compared to those of 6-fold coordinated V^{4+} ion (0.72 Å). Similar results were obtained for other 3d impurities in SnO_2.[17,18,39,41,68]

The formation of an interstitial V site induces, in addition to the structural distortions described in Section 3.1, an increment of the volume cell of SnO_2 (the lattice parameters are increased by 1.6%, $a = 4.822$ Å, $c = 3.242$ Å). Also, the inclusion of an oxygen vacancy increases the volume cell (a and c are increased by 0.5%, $a = 4.763$ Å, $c = 3.204$ Å). In both cases, the increments of the lattice parameters are in poor agreement with the experimental results.

3.3. Electronic Structure: Band Gap and Density of States. Calculations performed using local or semi-local approximations for the XC potential (LSDA and GGA) correctly predict the semiconductor nature of SnO_2 but underestimate the band gap, as it is well known. LSDA and GGA predict a band gap in the range 2.1−2.3 eV for SnO_2,[48−51,76] in disagreement with experimental results (in the range 3.25−3.6 eV, refs 14, 23, 44, 74, 75). A simple and computationally inexpensive improvement of LSDA/GGA is the DFT + U method in the self-interaction correction (SIC) scheme.[77] The question that arises here is the value that must be assigned to the U parameter for a given atom and orbital. The linear response approach based on the density functional perturbation theory developed by Timrov et al.[78] and Cococcioni and de Gironcoli[79] predicts that the best value for U to be applied to the 4d-Sn orbitals is in the order of 5 eV. Based on this, we used an effective $U^{eff} = U − J = 5$ eV value with $J = 0$ and obtained a band gap of 2.5 eV for SnO_2, still in poor agreement with the experimental results. Further increments of the U value do not enhance the band gap value of SnO_2. Based on this discussion, we will "jump" from the LSDA/GGA approximations for the XC potential to TB-mBJ and HSE06 models omitting the DFT + U methodology.

TB-mBJ and HSE06 calculations predict a direct band gap at the Γ-point of 3.8 and 3.6 eV, respectively, in excellent agreement with the experimental results.[14,23] In Figure 3 we present, as starting point of the discussion, the total (Figure 3a) and the atom-resolved partial density of states (DOS) (p-DOS, Figure 3b) of SnO_2 obtained by TB-mBJ calculation. As can be seen in Figure 3b, the valence band of SnO_2 is essentially formed by O-2p states with small contributions of Sn-5s and Sn-5p states (a clear evidence of the ionic nature of the Sn−O bonds in SnO_2). Also, hybridization between O-2p and Sn-4d states is observed in the valence band (the Sn-4d and O−2S states form a narrow band located close to 9 eV below the bottom of the valence band). The bottom of the conduction band presents essentially Sn-5s character (these states are located in the energy range 4−9 eV), and the Sn-5p states are located at higher energies. All these results are in excellent agreement with previous results obtained in previous DFT-based results.[48,80]

After the discussion of the electronic structure of the undoped SnO_2, we can discuss the changes induced in the electronic structure of the host by the presence of the V impurities. As can be seen in Figure 4, the doped system $Sn_{1-x}V_xO_2$ retains the semiconducting nature of SnO_2 for all the V-concentrations studied. The band gap is still direct at the Γ-point, but the presence of the V atoms induces impurity levels just below the Fermi level and at the bottom of the
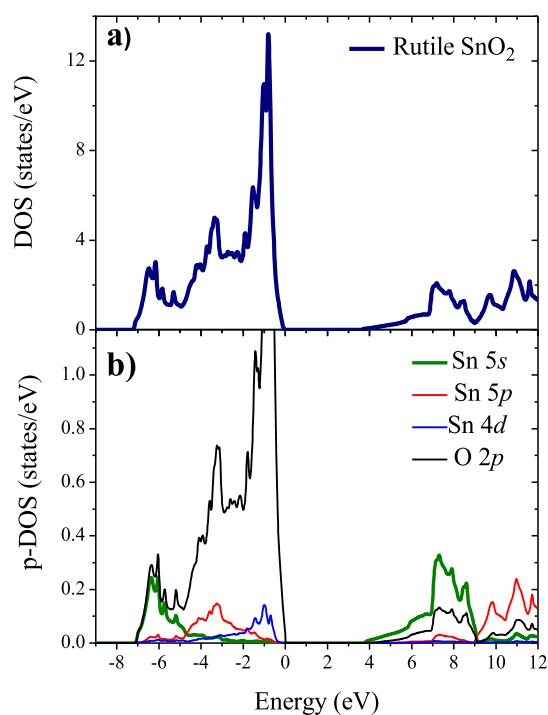
Figure 3. (a) Total DOS of pristine SnO_2 (TB-mBJ calculations). (b) Atom-projected DOS (p-DOS) of the dominant angular character of Sn and O. Energies are referred to the Fermi level (0.0 eV).
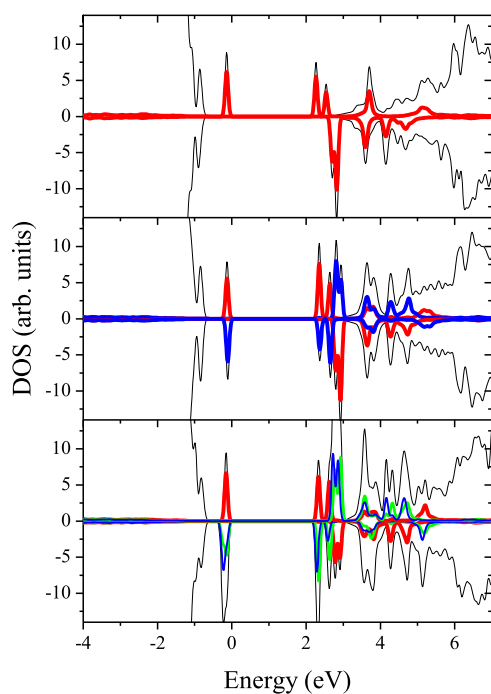

Figure 4. Total DOS of $Sn_{1-x}V_xO_2$ for the three V-concentration x studied: 0.042 (upper panel), 0.084 (middle), and 0.125 (bottom). Black lines correspond to the total DOS of $Sn_{1-x}V_xO_2$. Red, blue, and green lines correspond to the V1, V2, and V3 contributions, respectively. The results correspond to TB-mBJ calculations. Energies are referred to the Fermi level (0.0 eV). Positive/negative values indicate majority/minority spin channels.

conduction band, reducing the band gap, as can be seen in Figure 4. Based on the p-DOS projected in the V muffin-tin spheres, we find that the mentioned impurity states inside the

gap are originated by V-4d states hybridized with neighboring O1-2p and O2-2p states. Our results confirm those obtained by Salmani et al.[20] and refute the half-metallic character of $Sn_{1-x}V_xO_2$ reported in ref 17. This erroneous result can be attributed to the fact that this study was performed using the GGA approximation for the XC potential.

Different experimental determinations of the band gap of $Sn_{1-x}V_xO_2$ were reported in the literature.[44,74,75] For example, UV−visible diffuse reflectance spectroscopy shows a decrease of the band gap from 3.4 eV for pure SnO_2 to 2.2 eV for 10 at % V-doped SnO_2 ($x = 0.10$).[75] As can be seen in Figure 5 and
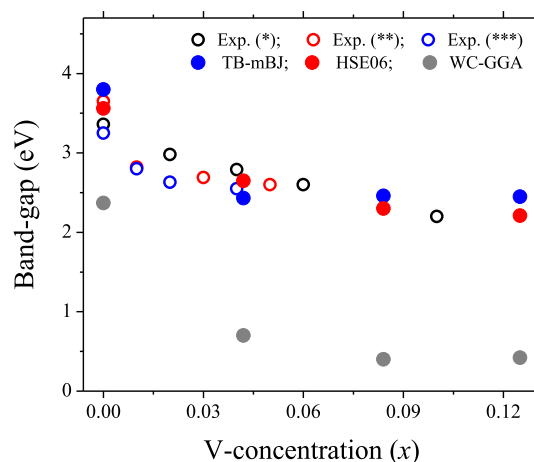

Figure 5. Band gap results obtained in the framework of WC-GGA, TB-mBJ, and HSE06 calculations as a function of the V-concentration x (*ref 75, **ref 74, and ***ref 44).

Table 4. Experimental and Calculated Band Gaps as a Function of the V-Concentration x

x	WC-GGA (eV) this work	TB-mBJ (eV) this work	HSE06 (eV) this work	exp. (eV)
0	2.30	3.8	3.56	3.25;[44] 3.36;[75] 3.6;[14,23] 3.65[74]
0.01				2.8;[44] 2.82[74]
0.02				2.63;[43] 2.98[75]
0.03				2.69[74]
0.04				2.56;[44] 2.79[75]
0.042	0.70	2.43	2.65	
0.05				2.60[74]
0.06				2.6[75]
0.084	0.40	2.46	2.3	
0.1				2.2[75]
0.125	0.42	2.45	2.21	

Table 4, TB-mBJ and HSE06 potentials predict a reduction of the band gap from 3.6 eV ($x = 0.0$, pure SnO_2) to 2.2 eV ($x = 0.125$). This theoretical trend and the band gap values as a function of x are in excellent agreement with experimental results.[44,74,75] On the other hand, LSDA and GGA predict a reduction of the band gap but, as expected, underestimate the band gap of $Sn_{1-x}V_xO_2$.

We also performed an additional calculation, considering an extremely large V-concentration (50%, $x = 0.5$). This calculation was performed using the primitive unit cell of SnO_2. This unit cell contains two Sn atoms. One of these Sn

atoms was replaced by one V impurity to obtain $x = 0.5$. For this impurity concentration, the V levels form a band at the top of the valence band and the bottom of the conduction band (see Figure 6). The TB-mBJ calculations predict for this
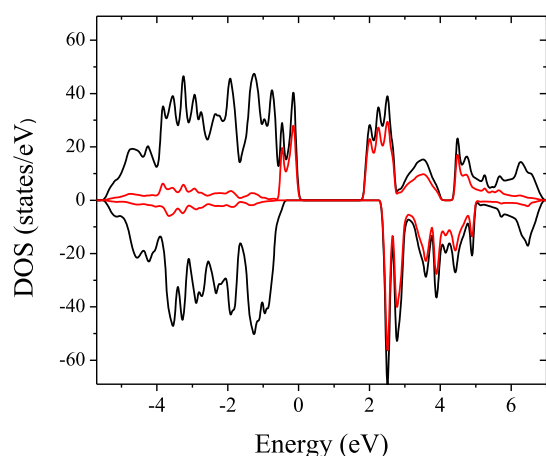

Figure 6. DOS of $Sn_{1-x}V_xO_2$ for $x = 0.50$. Black lines correspond to $Sn_{1-x}V_xO_2$. Red line corresponds to the total V contribution. The results correspond to TB-mBJ calculations. Energies are referred to the Fermi level (0.0 eV). These calculations were performed using the primitive unit cell of SnO_2. This unit cell contains two Sn atoms. One of these Sn atoms was replaced by one V impurity to obtain $x = 0.5$. Positive/negative values indicate majority/minority spin channels.

(unrealistic) V-concentration that the doped system is still a semiconductor with a band gap in the order of 1.6 eV (Figure 5). All these results show that the band gap of SnO_2 can be tuned by means of an appropriate doping with vanadium.

Finally, the formation of an interstitial V site reduces the band of the system to 1.3 eV. In the case of V-doped SnO_2 with an oxygen vacancy, the minimum band gap is in the order of 0.7 eV. In both cases, these results are in poor agreement with the experimental ones.

3.4. Hyperfine Interactions at the Sn and V Sites of $Sn_{1-x}V_xO_2$. The EFG tensor is a magnitude extremely sensitive to small changes in the asymmetry of the electronic charge density in the sub-nanoscopic environment of the Mössbauer probe. For this reason, the comparison of experimentally determined Δeq values and *ab initio* results is of fundamental importance for the validation of the structural and electronic modeling of the system under study.

In 2018, Ferrari et al.[45] reported the hyperfine characterization of $Sn_{1-x}V_xO_2$ nanoparticles obtained from ^{119}Sn-Mössbauer experiments performed at 300 K and ambient pressure ($x = 0.05, 0.075$, and 0.125). All the spectra exhibit a doublet which corresponds to a pure quadrupolar hyperfine interaction at the Sn sites. The hyperfine parameters IS and Δeq at the Sn sites derived from the fitting procedure are very similar to those obtained in pristine rutile SnO_2. The differences are a small increment of the IS (in the order of 0.01 mm/s) and an increment of Δeq (in the order of 0.1 mm/s, from 0.52 mm/s in the case of pristine SnO_2 to 0.64 mm/s for $Sn_{1-x}V_xO_2$, $x = 0.08$). Even small, these changes in the IS and Δeq are a clear indication of modifications in the structural and electronic environment of the Sn sites induced by the presence of the V impurities. It is important to note that the results reflect the average effects at the Sn sites originated by

the inclusion of V atoms at the cationic sites of the SnO_2 structure.

Before comparing theory−experiment, it is important to notice that the experiments were performed on nanoparticles with a minimum crystallite size of 100 Å. From the theoretical point of view, it is not possible to simulate a nanoparticle of this size. For this reason, we will compare experimental results obtained using nanoparticles as samples and bulk calculations. To validate this comparison, we performed calculations considering an affordable system that can give us information related to the effect of the reduced dimension of the nanoparticles. In our case, we studied (using the slab + vacuum geometry, the slab thickness employed was 25.44 Å, and a 10 Å vacuum was included) the (001), (110), and (110) surfaces of SnO_2. The aim of these calculations is not to determine the stable terminations of SnO_2. We just want to study how the hyperfine parameters at the Sn sites depend on the distance to the surface. Sn atoms located 7 Å below the surfaces reproduce the bulk results. Using this result and assuming a spherical nanoparticle with a radius of 50 Å, we determine that less than 0.2% of the Sn atoms "felt" the surface effects, giving support to the comparison of bulk calculations and nanoparticle experiments.

In Figure 7, we present our results for the IS and Δeq at the Sn sites of $Sn_{1-x}V_xO_2$ for each x value and for both WC-GGA
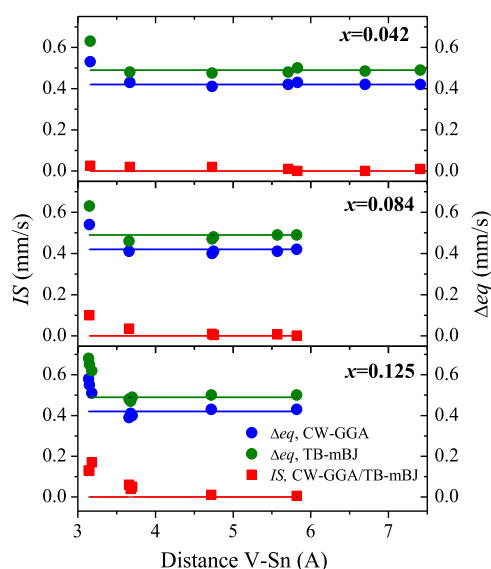

Figure 7. *Ab initio* results for the IS and Δeq at each Sn site of the 72-atom SC and each V-concentration x as a function of the V−Sn distance. Green and blue solid lines correspond to the Δeq values at the Sn sites in pristine SnO_2 predicted by TB-mBJ and WC-GGA potentials. The results for the IS obtained in each calculation differ by a value that is smaller than size of the squares. Solid red line corresponds to the IS at Sn sites in pristine SnO_2 (IS = 0.00).

and TB-mBJ approximations for the XC potential. In the theoretical study, contrary to the average IS and Δeq values obtained in the experiments, we can evaluate the hyperfine parameters at each Sn site. As can be seen in Figure 7, the values of IS and Δeq are very similar for the different Sn sites and V-concentrations except for the Sn nearest neighbors of the V impurities, which present slightly higher IS and Δeq values. The hyperfine interactions at Sn sites with V impurities beyond this first shell of cations (V−Sn separations larger than

3.2 Å) are "blind" to the substitution of a Sn atom of the lattice by a V impurity. When the V-concentration is increased, more Sn atoms have V atoms in the first cation coordination shell and, in consequence, a large effect in the hyperfine parameters is observed.

For a simplest comparison with the experimental results, we have considered the averaged values of the IS and Δeq over the different Sn sites for each concentration. As can be seen in Figure 8, our DFT results are in very good agreement with the
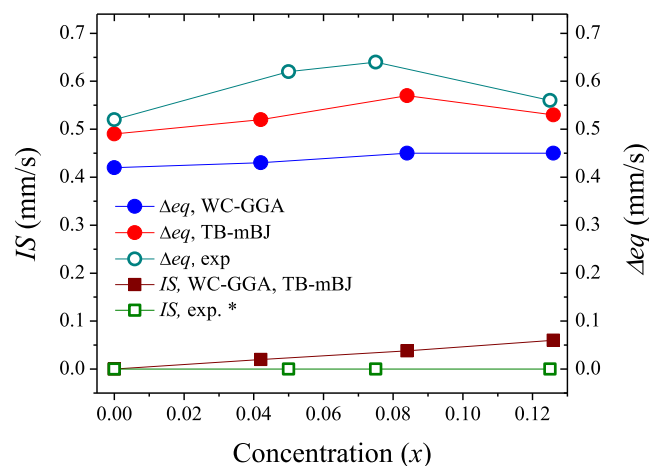

Figure 8. IS and Δeq values obtained in ^{119}Sn-Mössbauer spectroscopy at room temperature and ambient pressure and average *ab initio* predictions as a function of the V-concentration x. Solid green line corresponds to the IS at Sn sites in pristine SnO$_2$ (IS = 0.00) (*ref 45).

experimental ones and correctly reproduce the experimental trends of IS and Δeq at the Sn sites as a function of the V-concentration x.

To get a deeper understanding on the role played by the V impurities in the hyperfine interactions at the Sn sites, we performed some additional calculations. As we mentioned in the initial paragraph of this section, the EFG at the Sn sites strongly depends on fine details of the symmetry of the charge distribution around the Sn nucleus, which in turn reflects the Sn chemistry with its neighborhood and the Sn-ONN bond lengths. Since the substitution of Sn atoms by V ones induces structural distortions in the SnO$_2$ lattice, it is interesting to separate the electronic and structural effects induced by V in the hyperfine parameters at the sites of its Sn nearest neighbors. To do that we evaluate the hyperfine parameters at the Sn cation first neighbors of V (SnNN) in the case of the equilibrium structure of Sn$_{1-x}$V$_x$O$_2$ for x = 0.042 (1 V atom in the 72-atom SC, for a simplest discussion, we will focus on this case and the WC-GGA calculations). The hyperfine parameters obtained at the SnNN sites are V_{zz} = +7.7 × 10^{21} V/m^2, η = 0.299. Using eq 2, we obtained Δeq = 0.53 mm/s. This is our "reference site-state." After that we replaced the V impurity by the indigenous Sn atom keeping fixed the structure and calculated the hyperfine parameters at the same Sn sites. The results are V_{zz} = +7.9 × 10^{21} V/m^2, η = 0.244 (Δeq = 0.55 mm/s). Note that in both cases, the calculations are performed considering that the same structure and the hyperfine parameters are evaluated at the same reference site. The only difference between these calculations is that in the first case, the reference site has 1 V at 3.16 Å and one Sn at 3.24 Å. In the second case, the neighbors of the reference site are two Sn

atoms at 3.18 and 3.24 Å. As can be seen, the obtained hyperfine parameters are very similar in both cases, so Δeq at a given Sn site is not affected by the substituting Sn by V at 3.16 Å for a fixed structure. The variations of the hyperfine parameters at the Sn nearest neighbors of V are mainly originated in the structural distortions induced by the V impurity, so we could clearly separate here the structural and electronic effects on the EFG in a simple picture. The V impurity induced a structural distortion in the lattice that affects the local structure around its SnNN, and this distortion is at the origin of the changes in the IS and Δeq observed in Figure 7.

One of the isotopes of vanadium, ^{51}V, is a suitable probe for nuclear magnetic resonance spectroscopy (NMR) and, in consequence, ^{51}V solid-state NMR has become an important tool for the characterization of the local structure of vanadium sites in vanadium-based systems.[81] NMR can be used to obtain different information, that is, number of non-equivalent vanadium sites, the oxidation state and coordination number, and defects and distortions in the crystal structure can be revealed.[82−84] In consequence, ^{51}V-NMR experiments in Sn$_{1-x}$V$_x$O$_2$ samples could be of great importance to confirm (or discard) the results of our *ab initio* calculations. Unfortunately, no experimental ^{51}V-NMR results have been reported for this system till date.

Our results for the EFG tensor at V sites in Sn$_{1-x}$V$_x$O$_2$ are presented in Table 5. As can be seen, the EFG at the V sites is

Table 5. EFG Tensor Principal Components at the V Sites, V_{ii} (in 10^{21} V/m^2), for the Different V Concentrations x Studied[a]

XC potential	x	site	V_{xx}	V_{yy}	V_{zz}	η
WC-GGA	0.042	V1	−2.8	−4.8	+7.6	0.263
	0.084	V1	−2.6	−4.6	+7.2	0.271
		V2	−2.6	−4.6	+7.2	0.273
	0.125	V1	−2.5	−4.6	+7.1	0.298
		V2	−2.4	−4.3	+6.7	0.295
		V3	−2.5	−4.5	+7.0	0.278
TB-mBJ	0.042	V1	−4.4	−5.7	+10.1	0.133
	0.084	V1	−4.2	−5.5	+9.7	0.131
		V2	−4.2	−5.3	+9.8	0.132
	0.125	V1	−4.2	−5.5	+9.7	0.134
		V2	−4.0	−5.3	+9.3	0.139
		V3	−4.1	−5.5	+9.6	0.137

[a]In all cases, the EFG corresponds to the relaxed lowest energy structures for each x value.

almost irrespective of the V-concentration and the V-site considered. Based on this, we predict that one hyperfine interaction characterized by a V_{zz} value in the order of 7.0−7.6 × 10^{21} V/m^2 and η of about 0.28 will be observed according to the WC-GGA calculations. In the case of TB-mBJ, we predict V_{zz} in the order of 9.8 × 10^{21} V/m^2 and η of about 0.14. Clearly, a ^{51}V-NMR experiment could be very useful to determine which XC potential gives a more precise model for EFG tensor at the V sites and, in consequence, a more precise model for the electronic structure around its nucleus.

4. CONCLUSIONS

In this work, we studied the problem of a transition-metal impurity, vanadium, in rutile SnO$_2$ considering V-concentrations ranging from 0.042 to 0.125. In order to determine the

effect of the V-doping on the structural, electronic, magnetic, and hyperfine properties of $Sn_{1-x}V_xO_2$, we performed DFT-based calculations using two complementary methods: pseudopotential and plane waves and FP-LAPW, considering in both cases different approximations for the XC potential. Also, diverse V distributions and different collinear spin arrangements were computed with the aim to determine the structural and magnetic ground state for each V-concentration.

We found that V presents a 4+ oxidation state when it replaces Sn atoms of rutile SnO_2. Regarding magnetic properties, $Sn_{1-x}V_xO_2$ becomes spin-polarized. Spin polarization occurs mainly at the V sites and its nearest neighbor oxygens (ONN), which can be polarized up to 0.02 μ_B/ONN (a null magnetic moment is predicted at the Sn sites). These results are irrespective of the V-concentration and distribution. Our calculations indicate that paramagnetism is the magnetic ground state of V-doped SnO_2, in good agreement with results obtained in Monte Carlo simulations of the thermal dependence of the total magnetization and the magnetic susceptibility of $Sn_{1-x}V_xO_2$.

The replacement of indigenous Sn^{4+} atoms by V^{4+} ones induces a volume cell reduction that depends on the V-concentration, a result that is in very good agreement with the experimental ones. Also, the structural distortion around the V-impurity sites leads to a decrease of the V-ONN bond length of about 0.1 Å compared to the Sn-ONN bond lengths in pristine SnO_2. These results can be explained in terms of the smaller ionic radius of V^{4+} with respect to that of Sn^{4+}.

Based on the calculation of formation energies and the comparison with experimental results, we discard the formation of interstitial V sites and oxygen vacancies in $Sn_{1-x}V_xO_2$.

Concerning electronic properties, the V impurities induce impurity levels just below the Fermi level and at the bottom of the conduction band, reducing the band gap. This reduction of the band gap is in excellent agreement with the experimental results and refute the half-metallic nature of $Sn_{1-x}V_xO_2$ reported in the literature. The impurities levels are originated on the impurity d-states, which are hybridized with p-oxygen states. We also showed that TB-mBJ, an economic method (from the computational times and resources), correctly reproduces the band gap systematics as a function of the V-concentration.

Finally, our theoretical results correctly reproduce the hyperfine interactions measured by [119]Sn-Mössbauer spectroscopy in the studied range of V-concentrations. We also report here the hyperfine parameters at V sites. Due to the extreme sensitivity of the EFG tensor to small changes in the electronic structure around a probe atom, [51]V NMR experiments will be very valuable to confirm our structural, electronic, and magnetic model for $Sn_{1-x}V_xO_2$.

■ AUTHOR INFORMATION

Corresponding Author

    L. A. Errico − *Departamento de Física, Facultad de Ciencias Exactas, UNLP, 1900 La Plata, Argentina; Instituto de Física La Plata IFLP, CONICET, CCT, La Plata, 1900 La Plata, Argentina; Universidad Nacional Del Noroeste de La Pcia. de Buenos Aires (UNNOBA), Pergamino CP 2700, Buenos Aires, Argentina;* ⓞ orcid.org/0000-0002-9331-4222; Phone: (+54)92214764351; Email: errico@fisica.unlp.edu.ar

Authors

    H. H. Medina Chanduví − *Departamento de Física, Facultad de Ciencias Exactas, UNLP, 1900 La Plata, Argentina*

    A. M. Mudarra Navarro − *Departamento de Física, Facultad de Ciencias Exactas, UNLP, 1900 La Plata, Argentina; Instituto de Física La Plata IFLP, CONICET, CCT, La Plata, 1900 La Plata, Argentina*

    V. Bilovol − *Facultad de Ingeniería, Laboratorio de Sólidos Amorfos, Universidad de Buenos Aires, C1063ACV Buenos Aires, Argentina; Instituto de Tecnologías y Ciencias de la Ingeniería "Hilario Fernández Long" (INTECIN), CONICET-Universidad de Buenos Aires, C1063ACV Buenos Aires, Argentina*

    A. V. Gil Rebaza − *Departamento de Física, Facultad de Ciencias Exactas, UNLP, 1900 La Plata, Argentina; Instituto de Física La Plata IFLP, CONICET, CCT, La Plata, 1900 La Plata, Argentina; Grupo de Estudio de Materiales y Dispositivos Electrónicos (GEMyDE), CONICET, Universidad Nacional de La Plata UNLP, 1900 La Plata, Argentina*

Complete contact information is available at:
https://pubs.acs.org/10.1021/acs.jpcc.1c02285

Author Contributions

All images in figure graphics are original and have been fully created by the authors. H.H.M.C.: formal analysis, writing—review and editing, and investigation. A.M.M.N.: conceptualization, methodology, formal analysis, writing—review and editing, and investigation. V.B.: conceptualization, writing—original draft, writing—review and editing, formal analysis, and investigation. L.A.E.: project administration, conceptualization, supervision, methodology, writing—original draft, writing—review and editing, formal analysis, and investigation. A.V.G.R.: conceptualization, methodology, supervision, writing—original draft, writing—review and editing, formal analysis, and investigation.

Notes

The authors declare no competing financial interest.

■ ACKNOWLEDGMENTS

■ REFERENCES

(1) McCluskey, M. D.; Haller, E. E. *Dopants and Defects in Semiconductors*; Taylor & Francis Group: Florida, USA, 2012.

(2) Dierolf, V.; Ferguson, I. T.; Zavada, J. M. *Rare Earth and Transition Metal Doping of Semiconductor Materials, Synthesis, Magnetic Properties and Room Temperature Spintronics*; Woodhead Publishing: Cambridge, U.K., 2016.

(3) Ohno, H. Making nonmagnetic semiconductors ferromagnetic. *Science* **1998**, *281*, 951−956.

(4) Gregg, J. F.; Spintronics, J. F. a growing science. *Nat. Mater.* **2007**, *6*, 798−799.

(5) Ohno, H.; Stiles, M. D.; Dieny, B. Scanning the Issue. *Proc. IEEE* **2016**, *104*, 1782−1786.

(6) Bilovol, V.; Fontana, M.; Rocca, J. A.; Chanduví, H. H. M.; Navarro, A. M. M.; Rebaza, A. V. G.; Errico, L. A.; Liang, A.; Errandonea, D.; Ureña, A. M. Structural, vibrational and electronic properties in the glass-crystal transition of thin films Sb70Te30 doped with Sn. *J. Alloys Compd.* **2020**, *845*, 156307.

(7) Esquinazi, P. D.; Hergert, W.; Stiller, M.; Botsch, L.; Ohldag, H.; Spemann, D.; Hoffmann, M.; Adeagbo, W. A.; Chassé, A.; Nayak, S. K.; Ben Hamed, H. Defect-Induced Magnetism in Nonmagnetic Oxides: Basic Principles, Experimental Evidence, and Possible Devices with ZnO and TiO 2. *Phys. Status Solidi B* **2020**, *257*, 1900623.

(8) Minami, T. Transparent conducting oxide semiconductors for transparent electrodes. *Semicond. Sci. Technol.* **2005**, *20*, S35.

(9) Fritsch, D.; Ederer, C. Epitaxial strain effects in the spinel ferrites CoFe$_2$O$_4$ and NiFe$_2$O$_4$ from first principles. *Phys. Rev. B: Condens. Matter Mater. Phys.* **2010**, *82*, 104117.

(10) Caffrey, N. M.; Fritsch, D.; Archer, T.; Sanvito, S.; Ederer, C. Spin-filtering efficiency of ferrimagnetic spinels CoFe$_2$O$_4$ and NiFe$_2$. *Phys. Rev. B: Condens. Matter Mater. Phys.* **2013**, *87*, 024419.

(11) Das, S.; Jayaraman, V. SnO2: A comprehensive review on structures and gas sensors. *Prog. Mater. Sci.* **2014**, *66*, 112−255.

(12) Batzill, M.; Diebold, U. The surface and materials science of tin oxide. *Prog. Surf. Sci.* **2005**, *79*, 47−154.

(13) Gil Rebaza, A. V.; Errico, L. A.; Peltzer y Blancá, E. L.; Navarro, A. M. M. DFT-based study of the structural, electronic and hyperfine properties of the semiconducting alloys Sn1-xTixO2: HSE06 and non-regular TB-mBJ approach. *Mater. Chem. Phys.* **2019**, *237*, 121874. (and references there in)

(14) Godinho, K. G.; Walsh, A.; Watson, G. W. Energetic and Electronic Structure Analysis of Intrinsic Defects in SnO2. *J. Phys. Chem. C* **2009**, *113*, 439−448.

(15) Punnoose, A.; Hays, J.; Gopal, V.; Shutthanandan, V. Room-temperature ferromagnetism in chemically synthesized Sn1−xCoxO2 powders. *Appl. Phys. Lett.* **2004**, *85*, 1559−1561.

(16) Nomura, K.; Barrero, C. A.; Sakuma, J.; Takeda, M. Room-temperature ferromagnetism of sol-gel-synthesized Sn$_{1-x}$^{57}Fe$_x$O$_{2-\delta}$ powders. *Phys. Rev. B: Condens. Matter Mater. Phys.* **2007**, *75*, 184411.

(17) Wang, X. L.; Dai, Z. X.; Zeng, Z. Search for ferromagnetism in SnO2doped with transition metals (V, Mn, Fe, and Co). *J. Phys.: Condens. Matter* **2008**, *20*, 045214.

(18) Wang, X. L.; Zeng, Z.; Zheng, X. H. First-principles investigations of Co- and Fe-doped SnO$_2$. *J. Appl. Phys.* **2007**, *101*, 094H104.

(19) Kaur, J.; Shah, J.; Kotnala, R. K.; Verma, K. C. Raman spectra, photoluminescence and ferromagnetism of pure, Co and Fe doped SnO2 nanoparticles. *Ceram. Int.* **2012**, *38*, 5563−5570.

(20) Salmani, E.; Laghrissi, A.; Lamouri, R.; Rouchdi, M.; Dehmani, M.; Ez-Zahraouy, H.; Hassanain, N.; Mzerd, A.; Benyoussef, A. Theoretical study of electronic, magnetic and optical properties of TM (V, Cr, Mn and Fe) doped SnO$_2$: ab-initio and Monte Carlo simulation. *Opt. Quant. Electron.* **2018**, *50*, 85.

(21) Apostolov, A. T.; Apostolova, I. N.; Wesselinowa, J. M. A comparative study of the magnetization in transition metal ion doped CeO2, TiO2 and SnO2 nanoparticles. *Phys. E* **2018**, *99*, 202−207.

(22) Roy, S.; Luitel, H.; Sanyal, D. Magnetic properties of transition metal doped SnO2: A detailed theoretical study. *Comput. Condens. Matter* **2019**, *21*, No. e00393.

(23) Fröhlich, D.; Kenklies, R.; Helbig, R. Band-Gap Assignment in SnO2by Two-Photon Spectroscopy. *Phys. Rev. Lett.* **1978**, *41*, 1750.

(24) Dou, M.; Persson, C. Comparative study of rutile and anatase SnO2 and TiO2: Band-edge structures, dielectric functions, and polaron effects. *J. Appl. Phys.* **2013**, *113*, 083703.

(25) Toloman, D.; Popa, A.; Raita, O.; Stan, M.; Suciu, R.; Miclaus, M. O.; Biris, A. R. Luminescent properties of vanadium-doped SnO2 nanoparticles. *Opt. Mater.* **2014**, *37*, 223−228.

(26) Jiang, Q.; Zhang, L.; Wang, H.; Yang, X.; Meng, J.; Liu, H.; Yin, Z.; Wu, J.; Zhang, X.; You, J. Enhanced electron extraction using

SnO$_2$ for high-efficiency planar-structure HC(NH$_2$)$_2$PbI$_3$-based perovskite solar cells. *Nat. Energy* **2017**, *2*, 16177.

(27) Ellmer, K. Past achievements and future challenges in the development of optically transparent electrodes. *Nat. Photonics* **2012**, *6*, 809−817.

(28) Kikuchi, N.; Kusano, E.; Kishio, E.; Kinbara, A. Electrical and mechanical properties of SnO2:Nb films for touch screens. *Vacuum* **2002**, *66*, 365−371.

(29) Bahrami, B.; Khodadadi, A.; Kazemeini, M.; Mortazavi, Y. Enhanced CO sensitivity and selectivity of gold nanoparticles-doped SnO2 sensor in presence of propane and methane. *Sens. Actuators, B* **2008**, *133*, 352−356.

(30) Pearce, R.; Patterson, W. *Catalysis and Chemical Processes*; Leonard Hill Edit.: Glasgow, U.K., 1981.

(31) Nacimiento, F.; Alcántara, R.; Tirado, J. L. Polyacrylonitrile and cobalt-tin compounds based composite and its electrochemical properties in lithium ion batteries. *J. Alloys Compd.* **2009**, *485*, 385−390.

(32) Coey, J. M. D.; Douvalis, A. P.; Fitzgerald, C. B.; Venkatesan, M. Ferromagnetism in Fe-doped SnO2 thin films. *Appl. Phys. Lett.* **2004**, *84*, 1332−1334.

(33) Punnoose, A.; Hays, J. Possible metamagnetic origin of ferromagnetism in transition-metal-doped SnO2. *J. Appl. Phys.* **2005**, *97*, 10D321.

(34) Espinosa, A.; García-Hernández, M.; Menéndez, N.; Prieto, C.; de Andrés, A. Ferromagnetism in SnO$_2$-based multilayers: clustering of defects induced by doping. *Phys. Rev. B: Condens. Matter Mater. Phys.* **2010**, *81*, 064419.

(35) Stashans, A.; Puchaicela, P.; Rivera, R. DFT study of chromium-doped SnO2 materials. *J. Mater. Sci.* **2014**, *49*, 2904−2911.

(36) Bilovol, V.; Ferrari, S.; Saccone, F. D.; Pampillo, L. G. Effect of the dopant on the structural and hyperfine parameters of Sn0.95M0.05O2 nanoparticles (M: V, Mn, Fe, Co). *Mater. Res. Express* **2019**, *6*, 0850h6.

(37) Fang, L. M.; Zu, X. T.; Li, Z. J.; Zhu, S.; Liu, C. M.; Wang, L. M.; Gao, F. Microstructure and luminescence properties of Co-doped SnO2 nanoparticles synthesized by hydrothermal method. *J. Mater. Sci.: Mater. Electron.* **2008**, *19*, 868−874.

(38) Torres, C. E. R.; Errico, L.; Golmar, F.; Navarro, A. M. M.; Cabrera, A. F.; Duhalde, S.; Sánchez, F. H.; Weissmann, M. The role of the dopant in the magnetism of Fe-doped SnO2 films. *J. Magn. Magn. Mater.* **2007**, *316*, e219−e222.

(39) Mudarra Navarro, A. M.; Rodríguez Torres, C. E.; Cabrera, A. F.; Weissmann, M.; Nomura, K.; Errico, L. A. Ab Initio Study of the Ferromagnetic Response, Local Structure, and Hyperfine Properties of Fe-Doped SnO2. *J. Phys. Chem. C* **2015**, *119*, 5596−5603.

(40) Duhalde, S.; Vignolo, M. F.; Golmar, F.; Chiliotte, C.; Rodríguez Torres, C. E.; Errico, L. A.; Cabrera, A. F.; Rentería, M.; Sánchez, F. H.; Weissmann, M. Appearance of room-temperature ferromagnetism in Cu-doped TiO$_{2-\delta}$ films. *Phys. Rev. B: Condens. Matter Mater. Phys.* **2005**, *72*, 161313.

(41) Mudarra Navarro, A. M.; Rodríguez Torres, C. E.; Errico, L.; Nomura, K. The role of impurities and oxygen vacancies in the magnetic response of Fe$_x$Co$_y$Sn$_{1-x-y}$O$_2$. Experimental and ab initio study. *Mater. Chem. Phys.* **2021**, *257*, 123822.

(42) Fang, L. M.; Zu, X. T.; Li, Z. J.; Zhu, S.; Liu, C. M.; Zhou, W. L.; Wang, L. M. Synthesis and characteristics of Fe3+-doped SnO2 nanoparticles via sol-gel-calcination or sol-gel-hydrothermal route. *J. Alloys Compd.* **2008**, *454*, 261−267.

(43) Gu, F.; Wang, S. F.; Lü, M. K.; Zhou, G. J.; Xu, D.; Yuan, D. R. Photoluminescence Properties of SnO2 Nanoparticles Synthesized by Sol−Gel Method. *J. Phys. Chem. B* **2004**, *108*, 8119−8123.

(44) Letifi, H.; Litaiem, Y.; Dridi, D.; Ammar, S.; Chtourou, R. Enhanced photocatalytic activity of vanadium-doped SnO$_2$ nanoparticles in Rhodamine B degradation. *Adv. Condens. Matter Phys.* **2019**, *2019*, 2157428.

(45) Ferrari, S.; Bilovol, V.; Pampillo, L. G.; Grinblat, F.; Saccone, F. D.; Errandonea, D. Characterization of V-doped SnO2 nanoparticles at ambient and high pressures. *Mater. Res. Express* **2018**, *5*, 125005.

(46) Bolzan, A. A.; Fong, C.; Kennedy, B. J.; Howard, C. J. Structural studies of rutile-type metal dioxides. *Acta Crystallogr., Sect. B: Struct. Crystallogr. Cryst. Chem.* **1997**, *53*, 373−380.

(47) Hazen, R. M.; Finger, L. W. Bulk moduli and high-pressure crystal structures of rutile-type compounds. *J. Phys. Chem. Solids* **1981**, *42*, 143−151.

(48) Errico, L. A. Ab initio FP-LAPW study of the semiconductors SnO and SnO2. *Phys. B* **2007**, *389*, 140−144.

(49) Peltzer y Blancá, E. L.; Svane, A.; Christensen, N. E.; Rodríguez, C. O.; Cappannini, O. M.; Moreno, M. S. Calculated static and dynamic properties of β-Sn and Sn-O compounds. *Phys. Rev. B: Condens. Matter Mater. Phys.* **1993**, *48*, 15712−15718.

(50) Darriba, G. N.; Muñoz, E. L.; Errico, L. A.; Rentería, M. Ab Initio Study of Structural, Electronic, and Hyperfine Properties of n-type SnO2:Ta Semiconductor. *J. Phys. Chem. C* **2014**, *118*, 19929−19939.

(51) Miglio, A.; Saniz, R.; Waroquiers, D.; Stankovski, M.; Giantomassi, M.; Hautier, G.; Rignanese, G.-M.; Gonze, X. Computed electronic and optical properties of SnO2 under compressive stress. *Opt. Mater.* **2014**, *38*, 161−166.

(52) Sholl, D. S.; Steckel, J. A. *Density Functional Theory: A Practical Introduction*; John Wiley & Sons, Inc.: New Jersey, USA, 2009.

(53) Giannozzi, P.; Andreussi, O.; Brumme, T.; Bunau, O.; Buongiorno Nardelli, M.; Calandra, M.; Car, R.; Cavazzoni, C.; Ceresoli, D.; Cococcioni, M.; Colonna, N.; Carnimeo, I.; dal Corso, A.; de Gironcoli, S.; Delugas, P.; DiStasio, R. A., Jr.; Ferretti, A.; Floris, A.; Fratesi, G.; Fugallo, G.; Gebauer, R.; Gerstmann, U.; Giustino, F.; Gorni, T.; Jia, T. J.; Kawamura, M.; Ko, H.-Y.; Kokalj, A.; Küçükbenli, E.; Lazzeri, M.; Marsili, M.; Marzari, N.; Mauri, F.; Nguyen, N. L.; Nguyen, H.-V.; Otero-de-la-Roza, A.; Paulatto, L.; Poncé, S.; Rocca, D.; Sabatini, R.; Santra, B.; Schlipf, M.; Seitsonen, A. P.; Smogunov, A.; Timrov, I.; Thonhauser, T.; Umari, P.; Vast, N.; Wu, X.; Baroni, S. Advanced capabilities for materials modelling with Quantum ESPRESSO. *J. Phys.: Condens. Matter* **2017**, *29*, 465901.

(54) Sjöstedt, E.; Nordström, L.; Singh, D. J. An alternative way of linearizing the augmented plane-wave method. *Solid State Commun.* **2000**, *114*, 15−20.

(55) Madsen, G. K. H.; Blaha, P.; Schwarz, K.; Sjöstedt, E.; Nordström, L. Efficient linearization of the augmented plane-wave method. *Phys. Rev. B: Condens. Matter Mater. Phys.* **2001**, *64*, 195134.

(56) Blaha, P.; Schwarz, K.; Madsen, G.; Kvasnicka, D.; Luitz, J.; Laskowski, R.; Tran, F.; Marks, L. *WIEN2k, An Augmented Plane Wave plus Local Orbitals Program for Calculating Crystal Properties*; Schwarz, K., Ed.; Techn, Universität Wien: Austria, 2018.

(57) Prandini, G.; Marrazzo, A.; Castelli, I.; Mounet, N.; Marzari, N. Precision and efficiency in solid-state pseudopotential calculations. *npj Comput. Mater.* **2018**, *4*, 72.

(58) Wu, Z.; Cohen, R. E. More accurate generalized gradient approximation for solids. *Phys. Rev. B: Condens. Matter Mater. Phys.* **2006**, *73*, 235116.

(59) Perdew, J. P.; Burke, K.; Ernzerhof, M. Generalized gradient approximation made simple. *Phys. Rev. Lett.* **1996**, *77*, 3865−3868.

(60) Perdew, J. P.; Wang, Y. Accurate and simple analytic representation of the electron-gas correlation energy. *Phys. Rev. B: Condens. Matter Mater. Phys.* **1992**, *45*, 13244−13249.

(61) Heyd, J.; Scuseria, G. E.; Ernzerhof, M. Hybrid functionals based on a screened Coulomb potential. *J. Chem. Phys.* **2003**, *118*, 8207−8215.

(62) Heyd, J.; Scuseria, G. E.; Ernzerhof, M. Erratum: "Hybrid functionals based on a screened Coulomb potential" [J. Chem. Phys. 118, 8207 (2003)]. *J. Chem. Phys.* **2006**, *124*, 219906.

(63) Tran, F.; Blaha, P. Accurate band gaps of semiconductors and insulators with a semilocal exchange-correlation potential. *Phys. Rev. Lett.* **2009**, *102*, 226401.

(64) Schatz, G.; Weidinger, A. *Nuclear Condensed Matter Physics—Nuclear Methods and Applications*; Wiley: Chichester, U.K., 1996.

(65) Kaufmann, E. N.; Vianden, R. J. The electric field gradient in noncubic metals. *Rev. Mod. Phys.* **1979**, *51*, 161−214.

(66) Gütlich, P.; Bill, E.; Trautwein, A. X. *Mössbauer Spectroscopy and Transition Metal Chemistry*; Springer-Verlag: Berlin, Germany, 2011.

(67) Errico, L.; Lejaeghere, K.; Runco, J.; Mishra, S. N.; Rentería, M.; Cottenier, S. Precision of Electric-Field Gradient Predictions by Density Functional Theory and Implications for the Nuclear Quadrupole Moment and Its Error Bar of the 111Cd 245 keV 5/2+ Level. *J. Phys. Chem. C* **2016**, *120*, 23111−23120.

(68) Yahla, H.; Boukra, A.; Belhakem, M.; Lippens, P. E. First-principles calculations of the electronic structure and Mössbauer parameters of Sb-doped. *Solid State Commun.* **2009**, *149*, 2202−2206.

(69) Bader, R. F. W. *Atoms in Molecules: A Quantum Theory*; Oxford University Press: New York, USA, 1994.

(70) Kumarakrishnan, S.; Peterson, N. L.; Mason, T. O. Cation self-diffusion in disordered VOx. *J. Phys. Chem. Solids* **1985**, *46*, 1007−1014.

(71) Rogers, K. D. An X-ray diffraction study of semiconductor and metallic vanadium dioxide. *Powder Diffr.* **1993**, *8*, 240−244.

(72) Zibroc, I. P.; Filonenko, V. P.; Sidorov, V. A.; Lyapin, S. G. V$_{3.047}$O$_7$, a new high-pressure oxide with the simpsonite structure. *Inorg. Mater.* **2016**, *52*, 902−908.

(73) Filonenko, V. P.; Sundberg, M.; Werner, P.-E.; Zibrov, I. P. Structure of a high-pressure phase of vanadium pentoxide, β-V2O5. *Acta Crystallogr., Sect. B: Struct. Sci.* **2004**, *60*, 375−381.

(74) Reddy, C. V.; Babu, B.; Vattikuti, S. V. P.; Ravikumar, R. V. S. S. N.; Shim, J. Structural and optical properties of vanadium doped SnO 2 nanoparticles with high photocatalytic activities. *J. Lumin.* **2016**, *179*, 26−34.

(75) Ben Soltan, W.; Mbarki, M.; Ammar, S.; Babot, O.; Toupance, T. Structural and optical properties of vanadium doped SnO 2 nanoparticles synthesized by the polyol method. *Opt. Mater.* **2016**, *54*, 139−146.

(76) Borges, P. D.; Scolfaro, L. M. R.; Leite Alves, H. W.; da Silva, E. F., Jr. DFT study of the electronic, vibrational, and optical properties of SnO2. *Theor. Chem. Acc.* **2010**, *126*, 39−44.

(77) Anisimov, V. I.; Solovyev, I. V.; Korotin, M. A.; Czyżyk, M. T.; Sawatzky, G. A. Density-functional theory and NiO photoemission spectra. *Phys. Rev. B: Condens. Matter Mater. Phys.* **1993**, *48*, 16929−16934.

(78) Timrov, I.; Marzari, N.; Cococcioni, M. Hubbard parameters from density-functional perturbation theory. *Phys. Rev. B* **2018**, *98*, 085127.

(79) Cococcioni, M.; de Gironcoli, S. Linear response approach to the calculation of the effective interaction parameters in the LDA+U method. *Phys. Rev. B: Condens. Matter Mater. Phys.* **2005**, *71*, 035105.

(80) Fritsch, D.; Morgan, B. J.; Walsh, A. Self-Consistent Hybrid Functional Calculations: Implications for Structural, Electronic, and Optical Properties of Oxide Semiconductors. *Nanoscale Res. Lett.* **2017**, *12*, 19.

(81) Lapina, O. B.; Khabibulin, D. F.; Shubin, A. A.; Terskikh, V. V. Practical aspects of 51V and 93Nb solid-state NMR spectroscopy and applications to oxide materials. *Prog. Nucl. Magn. Reson. Spectrosc.* **2008**, *53*, 128−191.

(82) Mastikhin, V. M.; Lapina, O. B. *Vanadium Catalysts: Solid State NMR, Encyclopedia of Nuclear Magnetic Resonance*; Grant, D. M., Harris, R. K., Eds.; Wiley: New York, 1996; Vol. 8, pp 4892−4904.

(83) Lapina, O. B.; Shubin, A. A.; Khabibulin, D. F.; Terskikh, V. V.; Bodart, P. R.; Amoureux, J.-P. Solid-state NMR for characterization of vanadium-containing systems. *Catal. Today* **2003**, *78*, 91−104.

(84) Shubin, A. A.; Lapina, O. B.; Courcot, D. Characterization by solid state 51V NMR spectroscopy. *Catal. Today* **2000**, *56*, 379−387.